Korean J. Chem. Eng., **31**(9), 1598-1607 (2014)
DOI: 10.1007/s11814-014-0089-0

pISSN: 0256-1115
eISSN: 1975-7220

Functionalized nanostructured silica by tetradentate-amine chelating ligand as efficient heavy metals adsorbent : Applications to industrial effluent treatment

Afsaneh Shahbazi*, Habibollah Younesi,†, and Alireza Badiei*****

*Environmental Sciences Research Institute, Shahid Beheshti University, G.C., Tehran 1983963113, Iran
**Department of Environmental Science, Faculty of Natural Resources and Marine Sciences, Tarbiat Modares University, P. O. Box 46414-356, Noor, Iran
***School of Chemistry, College of Science, University of Tehran, P. O. Box 14155-6455, Tehran, Iran
(*Received 6 December 2013 • accepted 25 March 2014*)

Abstract−Organofunctionalized nanostructured silica SBA-15 with tri(2-aminoethyl)amine tetradentate-amine ligand was synthesized and applied as adsorbent for the removal of Cu^{2+}, Pb^{2+}, and Cd^{2+} from both synthetic wastewater and real paper mill and electroplating industrial effluents. The prepared materials were characterized by XRD, N_2 adsorption-desorption, TGA, and FT-IR analysis. The Tren-SBA-15 was found to be a fast adsorbent for heavy metal ions from single solution with affinity for Cu^{2+}, Pb^{2+}, than for Cd^{2+} due to the complicated impacts of metal ion electronegativity. The kinetic rate constant decreased with increasing metal ion concentration due to increasing of ion repulsion force. The equilibrium batch experimental data is well described by the Langmuir isotherm. The maximum adsorption capacity was 1.85 mmol g^{-1} for Cu^{2+}, 1.34 mmol g^{-1} for Pb^{2+}, and 1.08 mmol g^{-1} for Cd^{2+} at the optimized adsorption conditions (pH=4, T=323 K, t=2 h, C_0=3 mmol L^{-1}, and adsorbent dose=1 g L^{-1}). All Gibbs energy was negative as expected for spontaneous interactions, and the positive entropic values from 103.7 to 138.7 J mol^{-1} K^{-1} also reinforced this favorable adsorption process in heterogeneous system. Experiment with real wastewaters showed that approximately a half fraction of the total amount of studied metal ions was removed within the first cycle of adsorption. Hence, desorption experiments were performed by 0.3 M HCl eluent, and Tren-SBA-15 successfully reused for four adsorption/desorption cycles to complete removal of metal ions from real effluents. The regenerated Tren-SBA-15 displayed almost similar adsorption capacity of Cu^{2+}, Pb^{2+}, and Cd^{2+} even after four recycles. The results suggest that Tren-SBA-15 is a good candidate as an adsorbent in the removal of Cu^{2+}, Pb^{2+}, and Cd^{2+} from aqueous solutions.

Keywords: SBA-15, Heavy Metal Ion, Removal, Regeneration, Isotherm, Kinetic, Thermodynamics

INTRODUCTION

Industrial wastewater, especially surface finishing, petroleum refining, textiles, metal extraction, tannery, paints, pigment as well as the battery manufacturing, is a major source of heavy metal release to the environment. Removal of heavy metals is one of the major concerns in wastewater treatment because they are mostly toxic, resistant to biodegradation and have a propensity for bioaccumulation in living organisms, causing serious health problems. Methods proposed for heavy metal removal from wastewater include adsorption, chemical precipitation, membrane filtration, lime coagulation, ion-exchange, reverse osmosis and electrochemical processes [1]. Among them, adsorption is the treatment most widely applied due to its simple equipment, high efficiency, and inexpensive to operate [2-5]. Adsorption of heavy metals by mesoporous silica is a relatively recent method [6]. SBA-15 is one such promising mesoporous adsorbent because of its uniform, parallel, and cylindrical nano-channels with a large diameter, accompanied by complementary micropores within thick silicate walls, which facilitate mass diffusion and exhibit fast kinetics of chemical or physical processes [4,6,7]. Indeed, not only the pore-structure of such nano-structure sorbent but also the pore surface chemistry is of much importance for its affinity towards metal ions. Hence, post-synthetic grafting onto the mesoporous silica wall of organic groups with high density of donor species (e.g., N, O, S) which can form coordinate bonds with most toxic metal ions, has been an attractive route to developing new smart sorbents [4,5,8]. In recent years, there have been a large number of literature reports on removal of heavy metal cations by modified SBA-15 by different functionalities such as NH_2 [9], COOH [10], and SH [11]. Foreseeable advantages of these materials such as high hydrophilicity and flexibility of organic spacers together with their capability for chelating heavy metal ions make their use as metallic cation sorbents efficient.

In our earlier investigations, the functionalized SBA-15 by dendritic-amine groups were utilized as efficient adsorbent for heavy metal ions removal [12,13]. This study further examines the metal ion removal from simulated wastewater that contained copper, lead and cadmium ions using functionalized SBA-15 by tris(2-aminoethyl)amine, a tetradentate-amine chelating ligand, to optimize influence of various process parameters such as pH, nano-sorbent dosage, temperature, contact time and metal ion concentration. The feasibility of Tren-SBA-15 nano-sorbent for removing heavy metal ions was also evaluated for two real raw industrial effluents which were sampled from a paper mill and electroplating. The complete removal metal ions from these real effluents was achieved by sequential adsorption/desorption cycles.

†To whom correspondence should be addressed.
E-mail: hunesi@modares.ac.ir, hunesi@yahoo.com

MATERIALS AND METHODS

1. Chemicals and Reagents

The Pluronic P123 (PEO_{20}-PPO_{70}-PEO_{20}, M_{av}=5800) block copolymer non-ionic surfactant was purchased from Aldrich. Tetraethyl orthosilicate (TEOS, 98%), 3-chloropropyltrimethoxysilane (CPTES, 99%), tris(2-aminoethyl)amine ($N(CH_2CH_2NH_2)_3$, Tren, 98%), hydrochloric acid (HCl, 37%), toluene, methanol, $Pb(NO_3)_2$, $Cu(NO_3)_2$ and $Cd(NO_3)_2$ were provided by Merck (Germany).

2. SBA-15 Mesoporous Silica Synthesis and Functionalization

The synthesis of SBA-15 was similar to that described in the literature by using Pluronic P123 non-ionic surfactant as structure directing agent and using tetraethylorthosilicate as silica source under acidic conditions [7,12,14]. Briefly, P123 block copolymer (4 g) was dissolved in 2 M HCl (90 ml) and distilled water (2l ml) by stirring for 5 h at room temperature. Then, TEOS (6.4 g) was slowly added to that solution and stirred for 24 h at 40 °C. The mixture was aged in a sealed glass bottle at 100 °C for 24 h under static conditions. The mixture was allowed to cool at room temperature, and the white solid product was filtered, washed with distilled water for removing partial surfactant and dried. The solid was calcined in air at 600 °C for 6 h to completely remove the surfactant template, and a white powder (SBA-15) was obtained.

Surface modifications over SBA-15 were accomplished by a post-synthesis grafting method. The chloropropyl functionalization of SBA-15 was carried out using CPTES as the silylation reagent. In a typical surface modification process, calcined SBA-15 (5 g) was activated at 200 °C under vacuum for 8 h to remove surface humidity and refluxed in dry toluene (150 mL). Then CPTES (5.5 mL : 30.2 mmol) was slowly added to the mixture and refluxed at 110 °C for 24 h. The mixture was filtered and washed with toluene and any residual organosilane was removed by Soxhlet extraction over ethanol for 24 h. The obtained material was denoted as Cl-SBA-15. Subsequently, Cl-SBA-15 (7.5 mmol Cl, 5 g) was refluxed in dry toluene (150 mL) and Tren (9.0 mL : 60.0 mmol) was added to the mixture. This reaction mixture was refluxed at 110 °C for 24 h. Finally, the solid was filtered under a gentle argon flow, washed with toluene and any residual organic ligand was removed by Soxhlet extraction over ethanol for 24 h. The solid obtained was henceforth denoted as Tren-SBA-15 to be used as heavy metal sorbent. Tren-SBA-15 was kept under argon atmosphere until usage. All reactions described above were carried out under an inert atmosphere.

3. Materials Characterization

The materials (SBA-15, Cl-SBA-15, and Tren-SBA-15) were structurally characterized by powder X-ray diffraction, N_2 surface area analysis, Fourier transform infrared spectroscopy and thermal gravimetric analysis. The low-angle powder X-ray diffraction (XRD) patterns were recorded over a range of $0.5<2\theta<8$ degree on a Philips X'pert MPD diffractometer, equipped with a liquid nitrogen-cooled germanium solid-state detector, using Cu $K\alpha$ radiation (40 kV, 30 mA) at a step width of 0.02 degree. Nitrogen adsorption-desorption isotherms were measured at −196 °C using a BELsorp-mini II volumetric adsorption analyzer to determine the textural properties. All samples were degassed at 100 °C for 3 h under vacuum and argon gas flow before analysis. The specific surface area (S_{BET}) was evaluated using the Brunauer-Emmett-Teller (BET) method, and the pore size distribution (D_{BJH}) curves was calculated from the desorption branches of nitrogen isotherms applying the Barrett-Joyner-Halenda (BJH) method. The pore volume (V_{total}) was determined as the volume of liquid nitrogen adsorbed at a relative pressure of 0.995. The quantitative determination of the functional group content of the mesoporous silica was calculated by thermal gravimetric analysis (TGA) on a PL-Thermal Sciences PL-STA 1500, under an air flow starting at an ambient temperature up to 900 °C, using a ramp rate of 10 °C/min. Fourier transform infrared spectra (FT-IR) were recorded within a 600-4,000 cm^{-1} region on a Bruker Vector 22 infrared spectrophotometer.

4. Sorption Experiments: Isotherms, Kinetics, and Thermodynamics

A batchwise process was employed to study the sorption of Cu^{2+}, Pb^{2+} and Cd^{2+} from single aqueous solution onto the modified mesoporous silica Tren-SBA-15 at pH 4 and 25 °C. One important characteristic of a heavy metal sorbent is its sorption capacity at equilibrium. To determine this capacity for each metal ion, it was calculated as a function of the initial concentration of the metal ion (from 0.5 to 5 mmol L^{-1}) in a suspension of 50 mg of sorbent in 50 mL of a single metal solution. The sorption experiment was allowed to proceed by stirring overnight to let sorption sufficient time to reach equilibrium. Each sample was finally filtered through a 0.2 μm polypropylene syringe, and the concentration of the freely dissolved metal ions in the filtrate was analyzed by an atomic absorption spectrophotometer (Philips PU9400X, AAS, USA). To fit the linear calibration range, some samples were diluted with 5% HNO_3.

Another important characteristic of the prepared material is its sorption velocity in regard to the conditions and the time it takes for the particular ion under investigation, i.e., Cu^{2+}, Pb^{2+} or Cd^{2+}, to reach equilibrium. To determine the rate and the kinetics model of the sorption process, some sorbent (1 g L^{-1}) was suspended into 250 mL of a single metal solution with a concentration of 0.5, 2 and 3 mmol L^{-1}, and the concentration of the freely dissolved metal ions was determined by sampling at suitable time intervals from 2 min to 24 h to recognize the effect of ion concentration on sorption velocity.

Furthermore, the effect of temperature on the sorption of heavy metal ions onto Tren-SBA-15 was investigated by preparing a suspension of the sorbent (1 g L^{-1}) in 50 mL of a each single metal solution (3 mmol L^{-1}) and stirring it overnight on a temperature-controlled magnetic stirrer at various temperatures (10, 20, 30, 40, and 50 °C). Each sample was finally filtered through a 0.2 μm polypropylene syringe and the concentration of the freely dissolved metal ions in the filtrate was analyzed by an atomic absorption spectrophotometer.

In all experiments, the quantity of the metal ions adsorbed per unit mass of the Tren-SBA-15 was calculated by using the following equation:

$$q_e = \frac{(C_0 - C_e) \times V}{W} \quad (1)$$

where C_0 and C_e are the initial and equilibrium metal concentration (mmol L^{-1}), respectively, W is the mass of sorbent (g) and V is the volume of solution (L).

Note that the glassware was soaked in (1 : 1) HNO_3 overnight and cleaned with de-ionized water before starting each sorption experiment.

5. Application of Tren-SBA-15 Nano-sorbent in Real Effluent: Removal and Recovery

The feasibility of Tren-SBA-15 nano-sorbent for removing heavy

Table 1. Physicochemical characterization of raw industrial effluents from paper mill and electroplating units

Characteristics	Real effluents	
	Paper mill	Electroplating
pH (units)	3.5	4.2
EC (μS/cm)	1332	1527
Tem (°C)	30	26
Color	Dark yellow	Light yellow
TDS (mg/L)	865	929
COD (mg/L)	2488.3	2800.5
BOD (mg/L)	1150.6	90.2
Ca^{2+} (mg/L)	100.8	98.5
Mg^{2+} (mg/L)	87.9	67.9
Cu^{2+} (mg/L)	11.03	8.15
Pb^{2+} (mg/L)	30.94	6.94
Cd^{2+} (mg/L)	9.71	48.64

metal ions was evaluated for two real raw industrial effluents which sampled from paper mill and electroplating industries located in Tehran, Iran. The physicochemical characteristics of effluents, such as, pH value, electrical conductivity (EC), total dissolved solid (TDS), biochemical oxygen demand (BOD), chemical oxygen demand (COD), Ca^{2+}, Mg^{2+}, Cu^{2+}, Cd^{2+} and Pb^{2+} were analyzed promptly after collection and summarized in Table 1. Both types of real wastewater had a low pH, high levels of TDS and almost high contaminations of Cd^{2+}, Cu^{2+}, and Pb^{2+}. The results obtained from previous optimization adsorption experiments (sorbent dosage of 0.1 g L^{-1}, pH of 4, and temperature of 50 °C) were conducted for removal of heavy metal ions from real wastewaters. Because the regenerability of adsorbents is one of the its criteria characteristics due to make the treatment process more economical, the regenerability of Tren-SBA-15 was evaluated by collecting of sorbent after first cycle treating of real effluent and regenerating for ion removal from treated effluent. The eluent used for the regeneration of the sorbent was 0.3 M HCl [12]. Sequenced cycles of adsorption-desorption were continued until the heavy metal ions concentration was decreased to not detectable limit in treated effluent. The heavy metal recovery was calculated by the following equation:

$$\text{Recovery} = \frac{\text{Amount of metal ion desorbed}}{\text{Amount of metal ion adsorbed}} \times 100$$

RESULTS AND DISCUSSION

1. Characterization

The XRD pattern of SBA-15 showed the (1 0 0), (1 1 0) and (2 0 0) reflections, typical of an ordered mesoscopic structured silica, which exhibit the two-dimensional hexagonal symmetry array of the nanochannels (Fig. 1(a)). Cl-SBA-15 and Tren-SBA-15 are also characterized by the same pattern (Fig. 1(b)), indicating that neither the chloropropyl-functionalization nor the grafting of Tren affected the structural integrity of SBA-15. The intensity of the dominant peak at 2θ=0.98, attributed to the (1 0 0) diffraction peak [7], decreased during the surface modification steps due to the reduction in the scattering intensity of the silica wall after modifications [14]. The

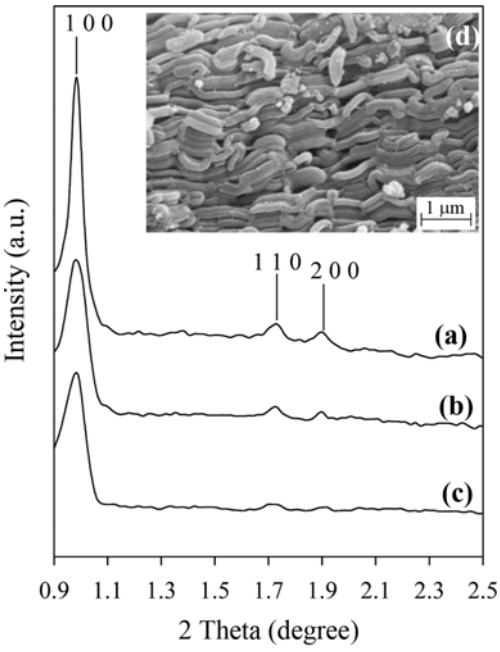

Fig. 1. Low-angle XRD patterns of (a) SBA-15, (b) Cl-SBA-15, and (c) Tren-SBA-15; and (d) SEM image of SBA-15.

SEM images (Fig. 1(d)) reveal that SBA-15 consists of many rope-like domains with a relatively uniform length of 1 μm, which morphology is in good agreement with the SBA-15 morphology presented in previous reports [15]. Both the porosity and volumetric characteristics of the two materials were evaluated by volumetric analyses. The "type IV" N_2 adsorption-desorption isotherms with "H1-type" hysteresis, shown in Fig. 2, corresponding to condensation and evaporation steps are characteristic of periodic mesoporous materials [16]. These results clearly indicate that the mesoscopic

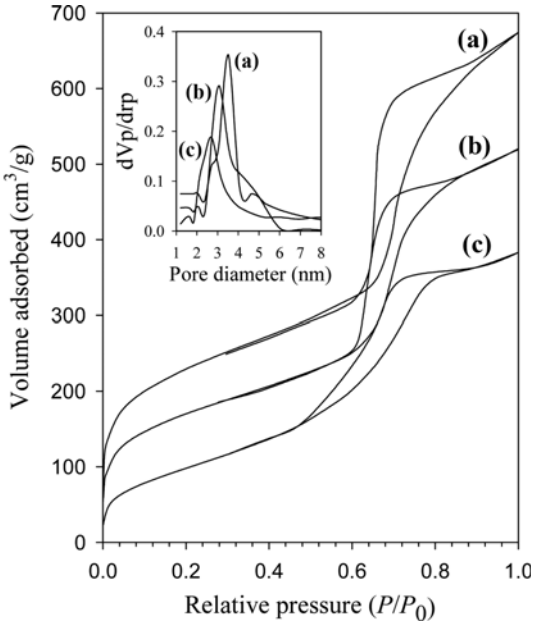

Fig. 2. Nitrogen adsorption-desorption isotherms and pore diameter distribution of (a) SBA-15, (b) Cl-SBA-15, and (c) Tren-SBA-15.

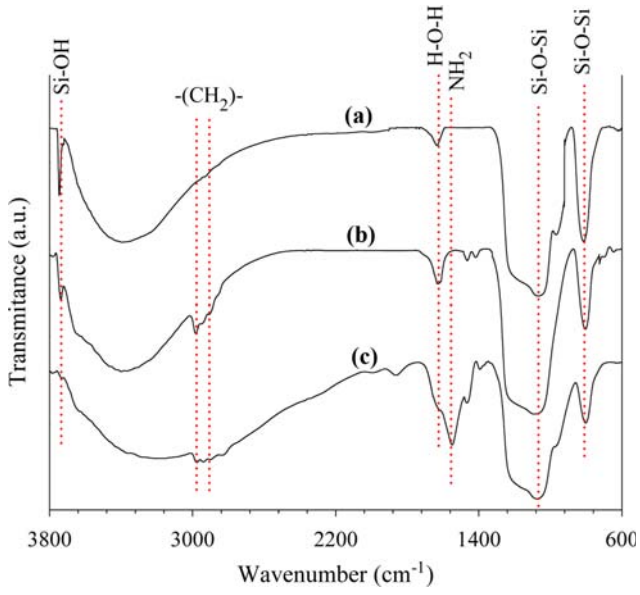

Fig. 3. FT-IR spectra of (a) SBA-15, (b) Cl-SBA-15, and (c) Tren-SBA-15.

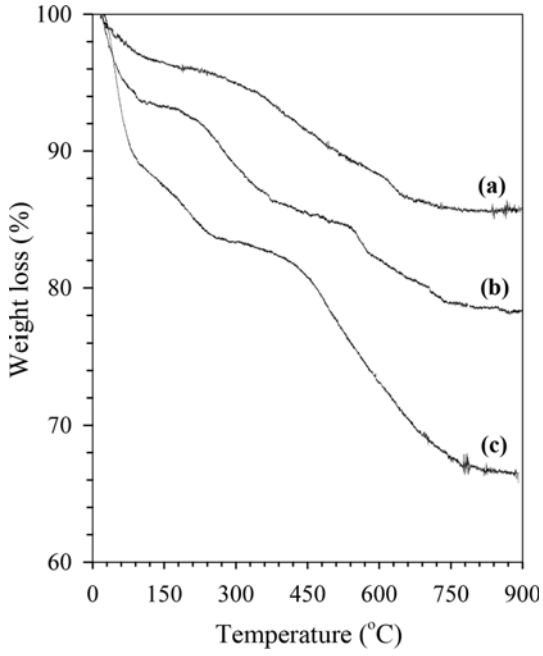

Fig. 4. Thermogravimetric curves of (a) SBA-15, (b) Cl-SBA-15, and (c) Tren-SBA-15.

structure was preserved during the surface modification, but the surface area and the pore volume and size decreased with increased modification. Cl-SBA-15 and Tren-SBA-15 exhibited significantly lower BET surface areas, i.e., 581 and 490 m^2/g, respectively, compared to 781 m^2/g for SBA-15, and also their pore volume of 1.40 and 1.02 cm^3/g and pore size of 5.42 and 4.01 nm, were lower than for SBA-15 (1.51 cm^3/g and 7.06 nm), confirming the notion that the surface modification takes place inside the silica nano-channels.

The incorporation of organic groups in the SBA-15 framework was confirmed by the FT-IR spectra (Fig. 3). In all the materials, the bands seen around 811 and 1,068 cm^{-1} are assigned to the typical symmetric and asymmetric stretching of Si-O-Si, due to the condensed silica network, whereas the strong band at 3,745 cm^{-1} is due to the presence of terminal silanol groups (Si-OH) located on the silica surface [5]. However, the disappearance of this peak in the Tren-SBA-15 sample (Fig. 3(c)) could be due to a reduced number of terminal silanol groups, caused by two possibilities, (a) hydrogen bonding between amine groups and silanols, (b) increasing adsorbed water because of the hydrophilic nature of the Tren ligand (Fig. 3(c)). This reduction is confirmed by the TGA results that showed the adsorbed water in the Tren-SBA-15 sample to be higher than in the Cl-SBA-15 and SBA-15 samples. The broad peak around 3,392 cm^{-1} is assigned to the O-H stretching vibration in SiO-H and HO-H of the absorbed water. In Fig. 3(b), the bands at 1,382 and 1,465 cm^{-1} are assigned to the $-CH_2$ bending vibration, while the peaks at 2,908 and 2,971 cm^{-1} are attributed to the C-H stretching vibrations in the methylene groups of the aliphatic chain, indicating the anchoring of CPTES on the silica surface [14]. In Fig. 3(c) the absorption band at 1,548 cm^{-1}, which clearly overlaps with the bending vibration of adsorbed H_2O, corresponds to the N-H bending vibration of $-NH_2$ groups. Moreover, the peaks at 2,836 and 2,977 cm^{-1} are assigned to C-H stretching vibrations of the methylene groups. Therefore, the FT-IR results confirm the anchoring of the functional groups on the SBA-15 silica surface.

The organic loading on the silica framework was estimated by TGA analysis, the results of which are shown in Fig. 4. In each curve the weight loss below 120 °C is due to the loss of the residual solvents and water. It seems that the weight loss in this range is 1.8 times higher for Tren-SBA-15 than for Cl-SBA-15 (11% *vs.* 6%). However, this difference might be due to the larger amount of water adsorbed by the Tren groups in the Tren-SBA-15 material. In other words, the amine groups extant in this ligand enhance the hydrophilic nature of the silica surface, which causes an increase in the adsorption of water. The weight loss between 120 and 800 °C was attributed to the organic moieties on the mesoporous silica surface. In Fig. 4(b), the gradual weight loss seen between 120 to 500 °C confirms the argument that the Cl-SBA-15 material is stable up to 500 °C, whereas Tren-SBA-15 (Fig. 4(c)) started to decompose at 400 °C. This means that the chloropropyl groups show a bit more thermal stability compared to the amine groups. Since in both materials some weight loss occurred between 120 and 800 °C, attributed to gradual silica matrix dehydroxylation, the weight loss between this ranges in the SBA-15 sample (Fig. 4(a)) was used as baseline for the silica dehydroxylation in order to correct the weight loss in these samples. Based on Fig. 4(b), the weight loss of the Cl-SBA-15 sample corresponds to the covalent anchor of 1.48 mmol/g of chloropropyl on the silica surface. From Fig. 4(c), a loading of about 0.95 mmol/g Tren groups on the silica surface was obtained, meaning that about 84% of the chloropropyl groups on the silica surface reacted with Tren.

Altogether, these characterization results of Tren-SBA-15 provide clear evidence of the fact that the organic functional groups were successfully grafted on the SBA-15 surface and the mesoprous ordering of the support was not affected by the chemical modification, revealing characteristics of a suitable metal ion sorbent.

2. Adsorption Isotherms

Based on the equilibrium adsorption results (Fig. 5(a)), Tren-SBA-15 showed a high sorption capacity of in range of 0.7-1.5 mmol g^{-1}

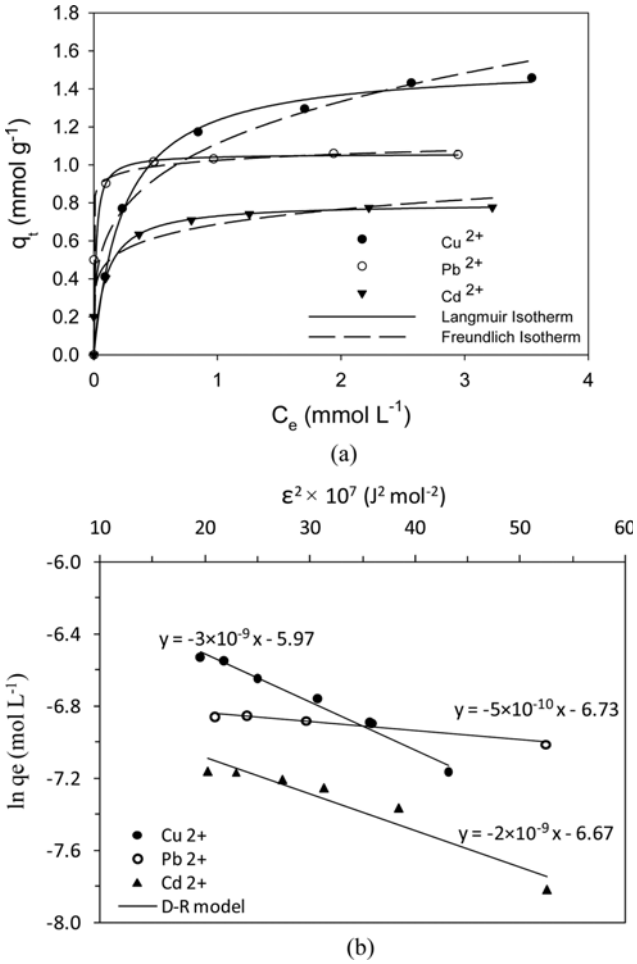

Fig. 5. Isotherm of heavy metal ions sorption onto Tren-SBA-15: (a) Langmuir and Freundlich models; (b) D-R model.

for metal ions studied. This high efficiency of Tren-SBA-15 for heavy metals removal is due to Tren chemical structure. In fact Tren on the SBA-15 surface makes a tridentate chelating ligand that forms stable complexes with transition metals, especially those in the 2^+ and 3^+ oxidation states [17].

As shown in Fig. 5(a), the sorption isotherms of the investigated metal ions on the oppositely charged surface of Tren-SBA-15 correspond to an L-type for Cu^{2+} and Cd^{2+} and to an H-type for Pb^{2+} in the Giles [18,19] system. The length of the plateau part of each isotherm indicates the difficulty of formation of a second layer because of the charge repulsion force between the adsorbed ions and those approaching from the solution [19], and this also indicates that the sorbent has a limited sorption capacity. Based on the sorbed ion equilibrium (q_e) presented in Fig. 5(a), the Tren-SBA-15 had an affinity for metal ions in a decreasing order of $Cu^{2+}>Pb^{2+}>Cd^{2+}$. A similar trend was reported to occur on amine-modified MCM-41 and activated carbon [20]. It is hardly reasonable to connect this metal selectivity order with a sieve effect, because all three ions have similar hydrated radii (around 0.4 nm) [21], clearly shorter than the functionalized-silica pore radii (with accessible pores of 2.0 nm). Based on the hard-soft-Lewis acid-base (HSAB) principle, the lower amount of sorption of cadmium compared to that of copper and lead can be explained by the greater hardness value of a cadmium ion (10.3 *vs.* 8.3 for copper and 8.5 for lead) [22], which causes lessening in its degree of softness and consequently also its potential to form covalent bonds with the amine groups on the silica surface. While the hardness value of both copper and lead ions are relatively similar, the different and higher absolute electronegativity value of copper ions compared to lead ions (28.5 *vs.* 23.6) [22] has to be considered as the responsible factor for its higher sorption value.

Within the concentration range studied, the isotherm behavior of Cu^{2+}, Pb^{2+} and Cd^{2+} sorption on Tren-SBA-15 were analyzed by the Langmuir, Freundlich, and Dubinin-Radushkevich (D-R) models.

The Langmuir model can be used to calculate some useful parameters, given by the following equation [23]:

$$q_e = \frac{q_m B C_e}{1 + b C_e} \tag{2}$$

where q_e is the equilibrium metal loaded by the sorbent (mmol g^{-1}) and q_m the maximum amount of ion that can be sorbed onto unit weight of sorbent (mmol g^{-1}), and C_e is the equilibrium metal concentration in the solution (mmol L^{-1}). The b constant (L $mmol^{-1}$) is related to the initial slope of the isotherm curve (Fig. 5(a)) and indicates the sorbent affinity.

The Freundlich model, which assumes a heterogeneous sorption, is expressed by the following equation:

$$q_e = K_f C_e^{1/n} \tag{3}$$

where K_f and n are considered to be relative indicators of sorption capacity and sorption intensity, respectively.

In Fig. 5(b) the equilibrium data were fitted to the Dubinin-Radushkevich (D-R) model, which is widely used to evaluate the nature of sorption. The D-R model is described by the following equation [24]:

$$\ln q_e = \ln q_m - \beta \varepsilon^2 \tag{4}$$

where q_m is the maximum amount of ions that can be sorbed onto unit weight of sorbent (mmol g^{-1}), β the constant related to sorption energy ($mol^2\ J^{-2}$), and ε the Polanyi potential (J mol^{-1}) which is calculated as function of the ions concentration at equilibrium:

Table 2. Calculated isotherm parameters for the sorption of metal ions on Tren-SBA-15

Metal ion	$q_{e,exp.}$ (mmol g^{-1})	Langmuir model			Freundlich model			D-R model		
		q_m (mmol g^{-1})	b (L $mmol^{-1}$)	R^2	K_f ($mmol^{(n-1)/n}\ g^{-1}\ l^{-1}$)	n	R^2	q_m (mmol g^{-1})	$-\beta$	R^2
Cu^{2+}	1.46	1.53	4.1	0.999	1.1	3.8	0.988	2.54	5×10^{-10}	0.981
Pb^{2+}	1.06	1.06	58.1	0.946	1.0	22.1	0.945	1.19	3×10^{-9}	0.942
Cd^{2+}	0.78	0.80	10.5	0.978	0.7	6.4	0.972	1.26	2×10^{-9}	0.924

$$\varepsilon = RT\ln\left(1+\frac{1}{C_e}\right) \quad (5)$$

where R is the gas constant (J K^{-1} mol^{-1}) and T the absolute temperature (K). The slope of the D-R plot (of $\ln q_e$ vs. ε^2) gives the β constant and the q_m value is obtained from the intercept of the plot.

The calculated Langmuir, Freundlich and D-R constants are listed in Table 2. The goodness of fit of the models to experimental data was evaluated by comparing the correlation coefficients R^2 and also taking into consideration q_e which was obtained from the experimental data. From Table 2, the isotherms of Cu^{2+}, Pb^{2+} and Cd^{2+} sorption on Tren-SBA-15 could be reasonably well described by the Langmuir model. The Langmuir model is developed to describe on the assumption that all adsorption sites on a structurally homogeneous adsorbent are identical and energetically equivalent. The results are coincident with similar studies [25-29] which used mesoporous silica for metal ion removal. According to the Langmuir theory, the adsorption takes place at specific homogeneous sites on the adsorbent. However, when a site is occupied by a solute, no further adsorption can take place at that site.

As shown in Fig. 5(a), the steepness of the initial slope of Pb^{2+} sorption isotherm which is related to the b constant (Table 2) and is much steeper than those for Cu^{2+} and Cd^{2+} isotherms, indicating a higher binding affinity of the sorbent for Pb^{2+} compared to Cu^{2+} and Cd^{2+}. However, the slope steadily falls with the rise in the metal concentration as vacant sites become more difficult to find with them progressively covering the surface. Lately, researchers have tested the sorption capacity of metal ions onto the functionalized mesoporous silica. For example, our previous study [12] showed that 1.9 mmol g^{-1} of Cu^{2+}, 0.6 mmol g^{-1} of Pb^{2+}, and 0.8 mmol g^{-1} of Cd^{2+} was sorbed by dendrimer-amine functionalized SBA-15 from single aqueous solutions. Benhamou et al. [5] observed a high degree of copper sorption (4.4 mmol g^{-1}) on DMDDA-MCM-41. A maximum sorption capacity around 0.8 mmol g^{-1} had been predicted by Aguado et al. [4] for Cu^{2+} with 2-aminoethylamino-propyl functionalized SBA-15. The noted variance of the published data may be caused not only by the physical properties (e.g., surface area and pore size) and chemical features (e.g., nature of ligand grafted onto the silica) of the used sorbent, but it may be related also to the initial conditions of the sorption experiment. Therefore, the different results are often difficult to compare.

3. Adsorption Kinetics

The influence of the initial metal concentration on the sorption rate was studied, keeping the sorbent dose at 1 g L^{-1} to show that an increase in this parameter reduces the sorption rate constant (Fig. 6, Table 3). The kinetic studies indicate that the time required to establish Cu^{2+}, Pb^{2+} and Cd^{2+} sorption equilibrium was not longer than 120 min, which was reasonably fast kinetics for the sorbent-sorbate interaction. This can be due to the accessibility of the ion binding sites on the surface of the sorbent. The kinetic data were modeled by pseudo-first-order (Eq. (6)) and pseudo-second-order (Eq. (7)) kinetic models and showed in Fig. 6.

$$q_t = q_e(1-\exp^{-k_1 t}) \quad (6)$$

$$q_t = \frac{k_2 q_e^2 t}{1+k_2 q_e t} \quad (7)$$

where t is the time (min), q_e (mmol g^{-1}) the equilibrium sorption capacity, k_1 (min^{-1}) and k_2 (g $mmol^{-1}$ min^{-1}) the pseudo-first-order and the pseudo-second-order rate constant.

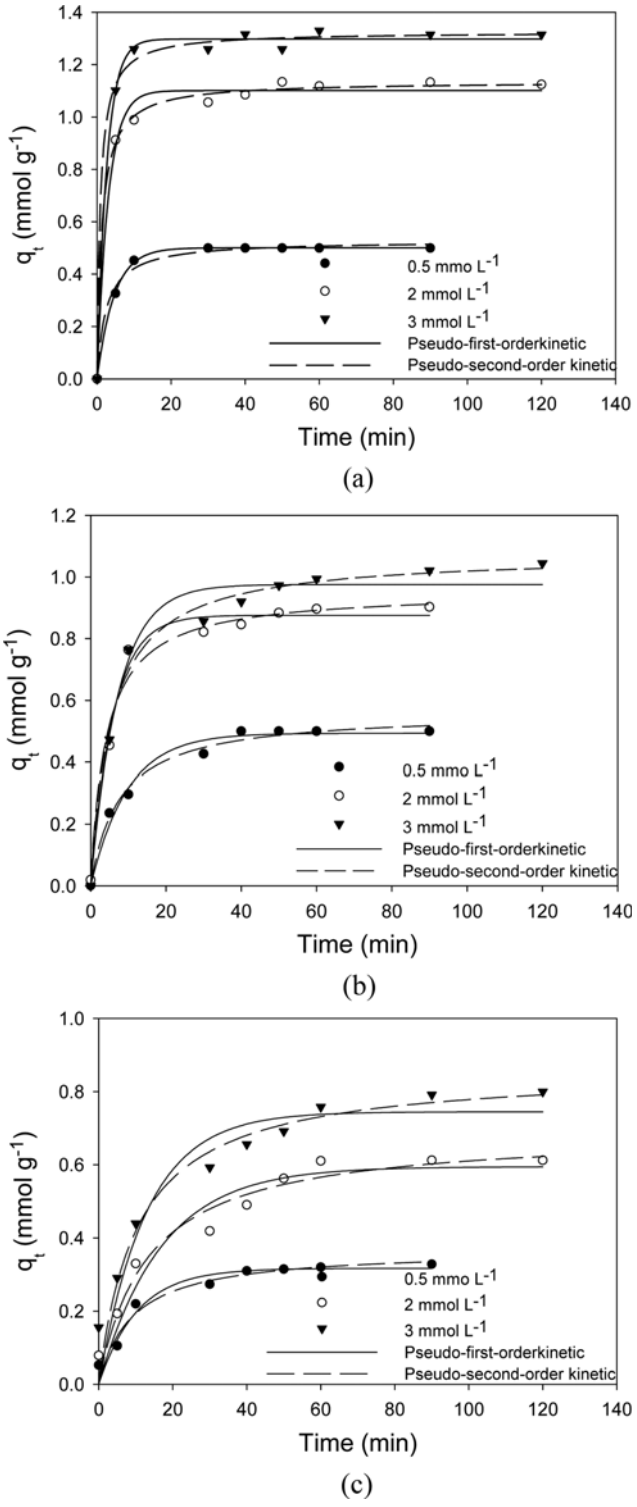

Fig. 6. Pseudo-first-order and pseudo-second-order kinetic models of (a) Cu^{2+}, (b) Pb^{2+} and (c) Cd^{2+} ions sorption onto Tren-SBA-15 (in the presence of 1 g L^{-1} Tren-SBA-15 at pH 4).

Calculated kinetic parameters for the sorption of studied metal ions onto Tren-SBA-15 are summarized in Table 3. From the Fig. 6 and Table 3, the kinetic sorption of Cu^{2+}, Pb^{2+}, and Cd^{+2} reasonably

Table 3. Calculated kinetic parameters for the sorption of metal ions on Tren-SBA-15

Metal ion	C_0 (mmol L^{-1})	$q_{e,exp.}$ (mmol g^{-1})	Pseudo-first-order kinetic			Pseudo-second-order kinetic		
			k_1 (min^{-1})	q_e (mmol g^{-1})	R^2	k_2 (g $mmol^{-1}$ min^{-1})	q_e (mmol g^{-1})	R^2
Cu^{2+}	0.5	0.50	0.377	0.5009	0.9900	1.599	0.53	0.9940
	2.0	1.12	0.325	1.01	0.9890	0.576	1.16	0.9990
	3.0	1.31	0.275	1.30	0.9960	0.540	1.34	0.9990
Pb^{2+}	0.5	0.50	0.802	0.49	0.9900	1.491	0.56	0.9940
	2.0	0.90	0.166	0.88	0.9860	0.250	0.95	0.9950
	3.0	1.02	0.137	0.98	0.9880	0.158	1.07	0.9940
Cd^{2+}	0.5	0.50	0.078	0.53	0.9920	0.298	0.56	0.9980
	2.0	0.61	0.009	0.62	0.9890	0.108	0.69	0.9950
	3.0	0.79	0.007	0.74	0.9820	0.106	0.86	0.9990

well fitted (R^2>0.994) to a pseudo-second-order kinetics. Quite a reasonable concord between the experimental and theoretical value of q_e (calculated from this model) was also obtained (Table 3). It means that initially most of the accessible sites on the outer (external) surface were easily available; in addition, the metal ion concentration was high, resulting in rapid sorption. With passing of time the sorption rate slowed down gradually until the equilibrium was reached owing to the decrease in both unoccupied sites and the ion concentration.

The influence of the initial metal concentration on the sorption rate showed that for example with a low load of lead ion (0.5 mmol L^{-1}), the equilibrium metal removal achieved within 30 min was 100% (k_2=1.5 g $mmol^{-1}$ min^{-1}). However, with a high lead ion concentration (3 mmol L^{-1}), the equilibrium metal removal attained in 90 min was 35% (k_2=0.16 g $mmol^{-1}$ min^{-1}). Since with an increased ion concentration the ion repulsion force also increased, so the metal ion itself became a potential competitor for occupying free sorption sites, resulting in decreasing kinetic rate constant. A similar behavior was reported for amine-functionalized SBA-15 [4,9]. The comparison between the Cu^{2+} Pb^{2+} sorption rate constants (Fig. 6) showed a faster sorption process (1.1- 4.5 times higher) for Cu^{2+}, which is probably due to a higher intrinsic affinity of the sorbent for Cu^{2+}. In the concentration range studied, the correlation between the kinetic rate constants of the metal ion sorption process and the initial metal ion concentration showed a non-linear trend (Fig. 6). Da'na et al. (2011) arrived at similar results for the sorption of copper to the amine-functionalized SBA-15 [9].

Generally, the sorption mechanism on porous sorbents is characterized by four stages: bulk diffusion, film diffusion, intra-particle diffusion and finally sorption of the solute on the pore surface at the sorption sites. In fact, one or more of these steps may limit the rate of sorption and determine the amount of sorption on the solid surface. Intra-particle diffusion is assumed to be slow and can therefore be a rate-limiting stage [30], expressed as:

$$q_t = k_{id} t^{1/2} + C \quad (8)$$

where k_{id} (mmol g^{-1} $min^{-1/2}$) is the intra-particle diffusion rate constant and C the y-intercept. Intra-particle diffusion was characterized by using the plot of q_t versus square root of time ($t^{1/2}$), described in Fig. 7. This plot provides clear evidence that the sorption process of Cu^{2+}, Pb^{2+} and Cd^{2+} consists of three stages, suggesting that the intra-particle diffusion might not be as the only rate limiting step for

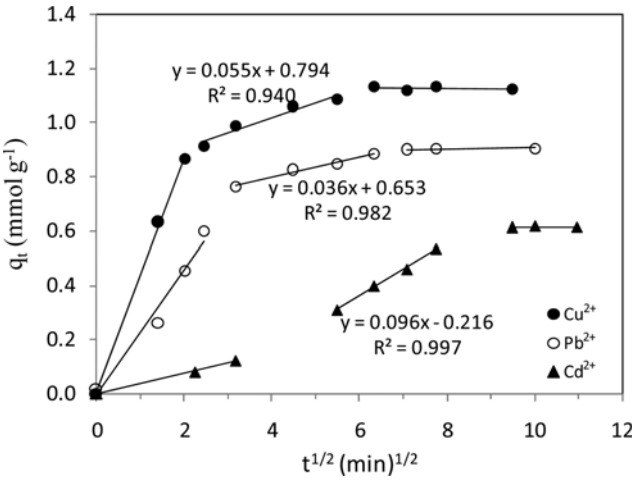

Fig. 7. Intra-particle diffusion kinetic plot of the sorption of metal ion (C_0=2 mmol L^{-1}) in the presence of 1 g L^{-1} Tren-SBA-15 at pH 4.

the whole reaction [9,31]. The slope of the linear portion indicates the rate of the sorption. The initial fast rate stage, finished in 5 min, was attributed to the diffusion of ions through the solution to the easily accessible sites on the external surface of the sorbent indicated an exterior mass transfer. With the saturation of the external sites, besides the decreasing concentration, intra-particle or pore diffusion took place according to the second linear portion of the plot. This stage was much slower than the initial stage. The third linear portion of the plot corresponds to the sorption at equilibrium. Comparing the three stages of sorption, the initial step was the fastest one for Cu^{2+} and Pb^{2+}. The slope of the second linear portion, attributable to the intra-particle diffusion rate constant, shows clearly that the intra-particle diffusion rate for Cd^{2+} is around two-times higher than that for Cu^{2+} and Pb^{2+}.

In summary, the bulk diffusion arises to restore the uniform adsorption monolayers, which oppose the film diffusion, and thus accelerate the film thinning. Film diffusion is related to viscosity; the surface tension is related to the intermolecular interaction of the solvent molecules. Furthermore, our experimental results illustrated that the presence of an additional flux may occur in parallel with diffusional mass transport through the mesopores. An intra-particle diffusion mechanism could be attributed significantly to the adsorp-

Table 4. Calculated thermodynamic parameters for the sorption of metal ions on Tren-SBA-15

Metal ion	Gibbs free energy							D-R model		
	ΔH (kJ mol^{-1})	ΔS (J mol^{-1} K^{-1})	ΔG (kJ mol^{-1})					R^2	E (kJ mol^{-1})	R^2
			283 K	293 K	303 K	313 K	323 K		303 K	
Cu^{2+}	24.88	138.76	−14.39	−15.77	−17.16	−18.55	−19.94	0.968	31.62	0.981
Pb^{2+}	20.89	120.89	−13.32	−14.53	−15.74	−16.94	−18.15	0.970	12.91	0.942
Cd^{2+}	16.64	103.76	−12.73	−13.76	−14.80	−15.84	−16.88	0.973	15.81	0.924

tion kinetics because of the higher concentration of the adsorbed metal ions on Tren-SBA-15. This means that the mobility of the adsorbate metal ions on the surface of Tren-SBA-15 was high in the pores. The experimental results indicated that intra-particle diffusion contributed more than 40% for Cu^{2+} and Pb^{2+} and 80% for Cd^{2+} ions of the total flux in the pores of the Tren-SBA-15 adsorbent.

4. Thermodynamics

The thermodynamic criteria such as the changes in Gibbs free energy (ΔG), in enthalpy (ΔH) and in entropy (ΔS) were determined using the following equations:

$$k_e = \frac{q_e}{C_e} \tag{9}$$

$$\ln k_e = \left(-\frac{\Delta H}{R}\right)\left(\frac{1}{T}\right) + \frac{\Delta S}{R} \tag{10}$$

$$\Delta G = \Delta H - T\Delta S \tag{11}$$

where k_e is the thermodynamic equilibrium constant (L g^{-1}) of the sorption system, T the temperature in Kelvin and R the universal gas constant (8.314 J mol^{-1} K^{-1}). ΔH (J mol^{-1}) and ΔS (J mol^{-1} K^{-1}) were obtained from the slope and intercept of plots of $\ln k_e$ versus 1/T. The calculated values of the thermodynamic parameters are summarized in Table 4. From the results, an increase in temperature shows the increase of the q_e and consequently that of the k_e. In fact, increasing the temperature is known to increase the rate of diffusion of the sorbate species across the external boundary layer and in the internal pores of the porous sorbent, owing to the decrease in the viscosity of the solution resulting in a higher equilibrium of the metal loaded by the sorbent. Another possible reason is the probable breaking of H-bonds between the amine groups and the hydroxyl groups on the silica surface, by the increased temperature releasing amine groups and leading to enhanced sorption capacity. The qualitative estimate of ΔH was found to be positive for all cases (Table 4) due to the endothermic nature of the sorption, which is in agreement with literature data for similar sorbents [9]. Despite the fact that the formation of a metal-amine coordination is assumed to be an exothermic event [32], the endothermic behavior observed is most likely due to a number of endothermic processes such as diffusion resistance or overcoming ion repulsion forces. The large positive metal-ligand heat changes (ΔH>16 kJ mol^{-1}) are characteristic of metal ion coordination with amino groups. The ΔH values obtained in the present study indicate rather weak ionic interaction between the sorbate and the Tren-SBA-15 sorbent and the metal removal seems to involve physisorption. The values of ΔS were found to be positive (Table 4), confirming the increased randomness of the ions bonding at the solid-solution interface during the sorption process that would cause increase in the entropy, besides reflecting an irreversibility of Cu^{2+}, Pb^{2+} and Cd^{2+} sorption on Tren-SBA-15. Another possibility that would cause increase in the entropy could be the liberation and dispersal of water molecules in the solution after the sorption process, of molecules previously bonded to the hydrated metal ion [33]. However, the magnitude of ΔS reflects the affinity of the metal ion for sorbent used. Based on the ΔS results (Table 4), the sorption affinity was in order of Cu^{2+}>Pb^{2+}>Cd^{2+}, which confirms the results obtained from the relevant part of the isotherm studies. The negative values of ΔG, which reflect the spontaneous nature and feasibility of the sorption process, were obtained within the temperature range studied. However, the higher magnitude of the negative values of ΔG at higher temperatures (e.g., 40 or 50 °C) implies the higher tendency and affinity of sorption combined with a more facile reaction. This may be due to the dehydration of metal ions, which facilitates their interaction with the chelating active sites.

Another equation that has been used to determine the possible sorption mechanism is the Dubinin-Radushkevich (D-R) equation. According to the D-R model, the mean free sorption energy E (J mol^{-1}) can be calculated using the following equation:

$$E = \frac{1}{\sqrt{-2\beta}} \tag{12}$$

where β is the activity coefficient obtained from Eq. (4).

The E value range from 8 to 16 kJ mol^{-1} obtained for Pb^{2+} and Cd^{2+} sorption (Table 4), suggested that the sorption of lead and cadmium ions onto functionalized-mesoporous silica mainly proceeded by binding surface functional groups [30], whereas for Cu^{2+} an E> 16 kJ mol^{-1} was observed, which suggested that the sorption was dominated by the intra-particle diffusion [30].

5. Real Industrial Effluent Treatment by Tren-SBA-15

The experimental results of adsorption/desorption cycles of heavy metal ions from paper mill and electroplating wastewaters are summarized in Table 5. As expected, the Tren-SBA-15 adsorption efficiency decreased significantly from the predicted behavior of Tren-SBA-15 based on complexity of real effluents. The fact that copper ions showed better affinity towards Tren-SBA-15 nano-sorbent than lead and cadmium which has been observed by synthetic wastewater was also proved by real effluents. The results showed that after first cycle adsorption process, the concentration of Ca^{2+}, Mg^{2+}, and TDS in untreated paper mill effluent was decreased of about 21% (from 865 to 683 mg/L), 10% (from 100 to 90 mg/L), and 8% (from 87 to 81 mg/L), respectively. Approximately, the same results were obtained for electroplating effluent. In fact, some of free cationic ions in the real wastewater adsorbed and occupied active sites onto Tren-SBA-15, leading to a lesser metal ion removal. Because the regenerability of adsorbent is one of the criteria characteristics

Table 5. Experimental results of adsorption/desorption cycles of heavy metal ions from paper mill and electroplating wastewaters by Tren-SBA-15

Real wastewater samples	Adsorption/ Desorption cycle	Metal ion	Before adsorption (mg/L)	After adsorption (mg/L)	Adsorption			Desorption
					R (%)	q_e (mg/g)	q_e (mmol/g)	Metal ion recovery (%)
Paper mill	First cycle	Cu^{2+}	11.03	6.54	40.7	44.9	0.71	99.2
		Pb^{2+}	30.94	19.13	38.2	118.1	0.57	98.6
		Cd^{2+}	9.71	7.70	20.7	20.1	0.18	99.1
	Second cycle	Cu^{2+}	6.54	3.20	51.1	33.4	0.53	97.5
		Pb^{2+}	19.13	11.42	40.3	77.1	0.37	97.0
		Cd^{2+}	7.7	6.11	20.6	15.9	0.14	98.4
	Third cycle	Cu^{2+}	3.2	n.d.*	100.0	32.0	0.50	98.0
		Pb^{2+}	11.42	4.92	56.9	65.0	0.31	97.2
		Cd^{2+}	6.11	4.64	24.1	14.7	0.13	98.0
	Fourth cycle	Cu^{2+}	-	-	-	-	-	95.0
		Pb^{2+}	4.92	n.d.	100.0	49.2	0.24	94.3
		Cd^{2+}	4.64	n.d.	100.0	46.4	0.41	96.8
Electroplating	First cycle	Cu^{2+}	8.15	3.70	54.6	44.5	0.70	99.0
		Pb^{2+}	6.94	1.05	84.9	58.9	0.28	98.0
		Cd^{2+}	48.64	40.51	16.7	81.3	0.73	99.5
	Second cycle	Cu^{2+}	3.7	n.d.	100.0	37.0	0.58	98.9
		Pb^{2+}	1.05	n.d.	100.0	10.5	0.05	98.1
		Cd^{2+}	40.51	32.16	20.6	83.5	0.75	99.1
	Third cycle	Cu^{2+}	-	-	-	-	-	-
		Pb^{2+}	-	-	-	-	-	-
		Cd^{2+}	32.16	23.28	27.6	88.8	0.79	96.6
	Fourth cycle	Cu^{2+}	-	-	-	-	-	-
		Pb^{2+}	-	-	-	-	-	-
		Cd^{2+}	23.28	15.03	35.4	82.5	0.74	94.0
	Fifth cycle	Cu^{2+}	-	-	-	-	-	-
		Pb^{2+}	-	-	-	-	-	-
		Cd^{2+}	15.03	7.10	52.8	79.3	0.71	93.8

*n.d.: not detected (lower than detection limit)

of sorbent due to make the treatment process more economical, particularly for industrial practice and provides the possibility for recovering metal ion from the liquid phase, hence the regenerability of Tren-SBA-15 was evaluated by collecting of sorbent after treating of real effluent and regenerating for ion removal from treated effluent. The treating results of paper mill effluent showed that Cu^{2+} was removed completely from wastewater after three adsorption/desorption cycles, while it occurred after four adsorption/desorption cycles for Pb^{2+} and Cd^{2+} (Table 5). However, for electroplating effluent, whole removal of Cu^{2+} and Pb^{2+}, Cd^{2+} and was obtained after two and five adsorption/desorption cycles, respectively. Altogether, the results show the feasibility and potential application of Tren-SBA- for the removal of MG from real industrial effluents.

CONCLUSIONS

The tris(2-aminoethyl)amine functionalized-SBA-15 with high density of nitrogen donor atoms was ascertained as a suitable sorbent for heavy metals removal from aqueous solution, exhibiting the highest sorption of 1.53, 1.06 and 0.80 mmol g^{-1} for Cu^{2+}, Pb^{2+} and Cd^{2+}, respectively, at pH 4. The isotherms of the metal ions studied can be described reasonably well by the Langmuir model. From kinetic studies the pseudo-second order model showed the best fit with the experimental data. The effect of the initial metal concentration on the sorption rate constant showed a negative correlation. The thermodynamic experiments provided clear evidence that the sorption process was endothermic ($\Delta H>0$) and spontaneous ($\Delta G<0$). The results show that Tren-SBA-15 can completely remove metal ions from real effluent after several-sequential adsorption/desorption cycles, and can therefore be used to treat industrial wastewater to a level that can be required for reuse applications. Hence, Tren-SBA-15 was found to be promising adsorbent for heavy metal ion removal from aqueous solution and industrial effluent due to its very high adsorption capacity, removal efficiency, and regenerability.

ACKNOWLEDGEMENTS

This research was financially supported by the Iranian Nanotechnology Initiative Council (INIC). The authors gratefully acknowledge Shahid Beheshti University and the University of Tehran (School

of Chemistry) for considerable laboratory supports, and science editor Ellen Vuosalo Tavakoli (University of Mazandaran) for her assiduous final editing of the English text.

REFERENCES

1. F. Fu and Q. Wang, *J. Environ. Manage.*, **92**, 407 (2011).
2. E. Da'na, N. De Silva and A. Sayari, *Chem. Eng. J.*, **166**, 454 (2011).
3. D. Perez-Quintanilla, I. del Hierro, M. Fajardo and I. Sierra, *J. Mater. Chem.*, **16**, 1757 (2006).
4. J. Aguado, J. M. Arsuaga, A. Arencibia, M. Lindo and V. Gascón, *J. Hazard. Mater.*, **163**, 213 (2009).
5. A. Benhamou, M. Baudu, Z. Derriche and J. P. Basly, *J. Hazard. Mater.*, **171**, 1001 (2009).
6. E. Da'na and A. Sayari, *Desalination*, **285**, 62 (2012).
7. D. Zhao, J. Feng, Q. Huo, N. Melosh, G. H. Fredrickson, B. F. Chmelka and G. D. Stucky, *Science*, **279**, 548 (1998).
8. A. Walcarius and C. Delacôte, *Anal. Chim. Acta*, **547**, 3 (2005).
9. E. Da'na, N. De Silva and A. Sayari, *Chem. Eng. J.*, **166**, 454 (2011).
10. M. C. Bruzzoniti, A. Prelle, C. Sarzanini, B. Onida, S. Fiorilli and E. Garrone, *J. Sep. Sci.*, **30**, 2414 (2007).
11. A. M. Burke, J. P. Hanrahan, D. A. Healy, J. R. Sodeau, J. D. Holmes and M. A. Morris, *J. Hazard. Mater.*, **164**, 229 (2009).
12. A. Shahbazi, H. Younesi and A. Badiei, *Chem. Eng. J.*, **168**, 505 (2011).
13. A. Shahbazi, H. Younesi and A. Badiei, *Can. J. Chem. Eng.*, **91**(4), 739 (2013).
14. A. Badiei, H. Goldooz and G. M. Ziarani, *Appl. Surf. Sci.*, **257**, 4912 (2011).
15. D. Zhao, J. Feng, Q. Huo, N. Melosh, G. H. Fredrickson, B. F. Chmelka and G. D. Stucky, *Science*, **279**, 548 (1998).
16. A. Badiei, H. Goldooz, G. M. Ziarani and A. Abbasi, *J. Colloid Interface Sci.*, **357**, 63 (2011).
17. D. A. House, *Ammonia & N-Donor Ligands, in: Encyclopedia of Inorganic Chemistry*, Wiley, New York (2006).
18. C. H. Giles, D. Smith and A. Huitson, *J. Colloid Interface Sci.*, **47**, 755 (1974).
19. G. Limousin, J. P. Gaudet, L. Charlet, S. Szenknect, V. Barthès and M. Krimissa, *Appl. Geochem.*, **22**, 249 (2007).
20. W. Yantasee, Y. Lin, G. E. Fryxell, K. L. Alford, B. J. Busche and C. D. Johnson, *Ind. Eng. Chem. Res.*, **43**, 2759 (2004).
21. E. R. Nightingale, *J. Phys. Chem.*, **63**, 1381 (1959).
22. R. G. Pearson, *Inorg. Chem.*, **27**, 734 (1988).
23. I. Langmuir, *J. Am. Chem. Soc.*, **40**, 1361 (1918).
24. B. P. Bering, M. M. Dubinin and V. V. Serpinsky, *J. Colloid Interface Sci.*, **38**, 185 (1972).
25. X. Xue and F. Li, *Micropor. Mesopor. Mater.*, **116**, 116 (2008).
26. A. Heidari, H. Younesi and Z. Mehraban, *Chem. Eng. J.*, **153**, 70 (2009).
27. Y. Kim, C. Kim, I. Choi, S. Rengaraj and J. Yi, *Environ. Sci. Technol.*, **38**, 924 (2003).
28. G. Li, Z. Zhao, J. Liu and G. Jiang, *J. Hazard. Mater.*, **192**, 277 (2011).
29. M. R. Awual, I. M. Rahman, T. Yaita, M. A. Khaleque and M. Ferdows, *Chem. Eng. J.*, **236**, 100 (2014).
30. M. E. Argun, S. Dursun, C. Ozdemir and M. Karatas, *J. Hazard. Mater.*, **141**, 77 (2007).
31. Y. Khambhaty, K. Mody, S. Basha and B. Jha, *Chem. Eng. J.*, **145**, 489 (2009).
32. E. Guibal, M. Jansson-Charrier, I. Saucedo and P. L. Cloirec, *Langmuir*, **11**, 591 (1995).
33. A. Kilislioglu and B. Bilgin, *Appl. Radiat. Isot.*, **58**, 155 (2003).